OPEN ACCESS



Three-dimensional Hybrid Simulation Results of a Variable Magnetic Helicity Signature at Proton Kinetic Scales

Bernard J. Vasquez¹⁰, Sergei A. Markovskii, and Charles W. Smith¹⁰

Space Science Center, University of New Hampshire, Durham, NH 03824, USA; bernie.vasquez@unh.edu, sergei.markovskii@unh.edu, charles.smith@unh.edu

*Received 2021 March 9; revised 2021 November 18; accepted 2021 November 19; published 2022 January 11

Abstract

Three-dimensional hybrid kinetic simulations are conducted with particle protons and warm fluid electrons. Alfvénic fluctuations initialized at large scales and with wavevectors that are highly oblique with respect to the background magnetic field evolve into a turbulent energy cascade that dissipates at proton kinetic scales. Accompanying the proton scales is a spectral magnetic helicity signature with a peak in magnitude. A series of simulation runs are made with different large-scale cross helicity and different initial fluctuation phases and wavevector configurations. From the simulations a so-called total magnetic helicity peak is evaluated by summing contributions at a wavenumber perpendicular to the background magnetic field. The total is then compared with the reduced magnetic helicity calculated along spacecraft-like trajectories through the simulation box. The reduced combines the helicity from different perpendicular wavenumbers and depends on the sampling direction. The total is then the better physical quantity to characterize the turbulence. On average the ratio of reduced to total is 0.45. The total magnetic helicity and the reduced magnetic helicity show intrinsic variability based on initial fluctuation conditions. This variability can contribute to the scatter found in the observed distribution of solar wind reduced magnetic helicity as a function of cross helicity.

Unified Astronomy Thesaurus concepts: Solar wind (1534); Interplanetary turbulence (830); Space plasmas (1544)

1. Introduction

Interplanetary turbulence is associated with a spectral magnetic helicity signature at proton kinetic scales. Magnetic helicity is the inner product the vector potential \boldsymbol{A} and the magnetic field \boldsymbol{B} averaged over some volume. The corresponding spectral magnetic helicity H_m is given by the inner product of the Fourier transform of \boldsymbol{A} and the conjugate of the transform of \boldsymbol{B} . The sign of spectral helicity gives the handedness of magnetic field variations. This can distinguish wave modes or correspond to nonlinear fluctuations.

The normalized magnetic helicity spectrum σ_m is defined as $kH_{\rm m}/P_B$, where k is a wavenumber, and P_B is the magnetic spectral energy at k. The value of σ_m varies between limits of -1 and 1.

A single spacecraft samples variations along one path. Without the availability of three-dimensional (3D) gradients of \boldsymbol{B} , \boldsymbol{A} cannot generally be determined. However, magnetic field data along the sampling path can provide a reduced magnetic helicity spectrum. The reduced spectrum corresponds to the magnetic helicity spectrum integrated for the plane of wavevectors that all have the same wavenumber along the sampling direction (Matthaeus et al. 1982). The observed value of normalized reduced magnetic helicity $\sigma_{m,\mathrm{red}}$ also varies between -1 and 1. In the normalization, k is based on the wavenumber of an advected fluctuation for spacecraft frequency ν and solar wind speed V_{SW} and is given by $k=2\pi\nu/V_{\mathrm{SW}}$.

The observed $\sigma_{m,\text{red}}$ values are found to be correlated with the rms normalized cross helicity σ_c , which is the correlation of fluctuating velocity and magnetic fields normalized by the sum

Original content from this work may be used under the terms of the Creative Commons Attribution 4.0 licence. Any further distribution of this work must maintain attribution to the author(s) and the title of the work, journal citation and DOI.

of kinetic and magnetic energy (Leamon et al. 1998; Hamilton et al. 2008; Smith et al. 2012; Markovskii et al. 2015; Vasquez et al. 2018). It, too, varies between -1 and 1. The rms value corresponds to large scales of the interval where the spectrum is calculated and is associated with fluctuations from the inertial range of the turbulence. For Alfvén wave modes in the long-wavelength limit, σ_c indicates the fraction of energy in wave modes with opposite senses of propagation relative to the background magnetic field B_0 . The fluctuations propagating outward from the Sun are identified as right handed according to the plasma physics convention if the magnetic helicity has the opposite sign compared to observed cross helicity and left handed if the sign is the same (Smith et al. 1983).

A fit with $\sigma_{m,red} = -0.41\sigma_c$ was found in the work of Leamon et al. (1998) so that the magnitude of $\sigma_{m,red}$ is always well removed from unity. The correlation and far less than unity magnitudes were interpreted to be the result of ion cyclotron and other forms of damping of the turbulence generated fluctuations. The sign of the helicity is consistent with right-handed kinetic Alfvén wave modes propagating away from the Sun. The smaller range of magnitudes was considered in Klein et al. (2014) to be due to a different fraction of outward and inward mode propagation in the kinetic range relative to that at larger scales (see also Howes & Quataert 2010; He et al. 2012).

The development of spectral magnetic helicity at kinetic scales in association with turbulence has been examined in two-dimensional (2D) hybrid numerical simulations with particle protons and fluid electrons (Markovskii & Vasquez 2013a, 2013b, 2016). The simulated fluctuations had wavevectors confined to the plane perpendicular to the background magnetic field. In these directions, a linear kinetic Alfvén wave cannot propagate. At the proton kinetic scales, a magnetic helicity signature develops with a peak when $\sigma_c \neq 0$. The magnitude and position of the peak varies with the sum of

the ratios of proton and electron plasma pressure to magnetic pressure β . A peaked form results from nonlinearity and differs from the behavior of a linear kinetic Alfvén wave. However, the sign of the magnetic helicity does agree with the right handedness of that mode.

From WIND observations, the results in Markovskii et al. (2015) and Markovskii & Vasquez (2016) show that there were signatures with peaks that were arguably at low enough spacecraft frequencies that aliasing did not affect them. Intervals from both slow and fast wind are well represented in the study. The mean properties of the peaks of helicity were consistent with the 2D simulation results. Fluctuations then appeared to be well described as having perpendicular wavevectors energized by a turbulent cascade and possessing nonlinear properties (consider also Woodham et al. 2019; Zhao et al. 2021).

In Vasquez et al. (2018) a wavelet method averaged over time of observation provided a clear organization to the relation between cross helicity and spectral magnetic helicity. The right-handed nature of the magnetic helicity was again found, and they focused on fits using the absolute value of the helicities. The fit function of the trend in magnitudes was $|\sigma_{m,\mathrm{red}}| = 0.3 |\sigma_{\rm c}|$. The distribution about the mean trend line was not dependent upon the obliquity angle θ_B between the sampling direction and background magnetic field. This could indicate that fluctuations have wavevectors that are associated with magnetic helicity over a wide range of angles. In this case, the 2D results in the perpendicular plane would be too limited to account for all observations. In addition, $|\sigma_{m,red}|$ was evaluated in Vasquez et al. (2018) for one 2D simulation case using a large series of sampling lines. The average determined, however, was higher than the expected mean based on observations. This too suggested that more than 2D results would be needed to explain the observed magnetic helicity.

Another possibility is that the signature has significant variability with respect to the parameters that have been identified, at least, on average to impact the value of helicity. Intervals where spectra were obtained were further subdivided in the work Vasquez et al. (2018), and spectra were recalculated for these subintervals. Variability was found in the signatures between the subintervals per interval and in the local parameters σ_c , β , and θ_B . Wavelets allow the signature to be examined as a function of time. In the works of He et al. (2011), Podesta & Gary (2011), and Bruno & Telloni (2015), wavelet spectra of helicity were found that did vary significantly with time and could be organized according to quasi-parallel and quasi-perpendicular bins with respect to the mean field at each scale.

In the present analysis, 3D simulations of quasi-perpendicular turbulence are carried out with different initial conditions. Magnetic helicity from simulation runs can be gyro averaged about the background magnetic field to obtain a so-called total magnetic helicity. This better represents the helicity signature for quasi-perpendicular turbulence in that the total evaluates helicity as a function of a single perpendicular scale. The reduced magnetic helicity, which can be obtained from observations, is also assessed but mixes perpendicular scales. The peak value of the reduced helicity will be shown to be about one-half of the total. A range of variability in both quantities is found. The range in the reduced helicity is consistent with observations so that the observed magnetic helicity signature is also consistent with a quasi-perpendicular

set of fluctuations. The 2D results correctly identified the mean parameters by which helicity varies. The differences about the mean arise from the intrinsic variability of the helicity signature for turbulent fluctuations.

The paper is organized as follows: Section 2 describes the simulation setup. The simulation results of the magnetic helicity signature for a range of conditions are presented in Section 3. Section 4 discusses and summarizes the results and conclusions.

2. Simulation Initial Conditions and Parameters

3D hybrid numerical simulations have been carried out with particle protons and a quasi-neutralizing, massless electron fluid to investigate the development of quasi-perpendicular turbulence. The employed numerical method is described in Terasawa et al. (1986) and Vasquez (1995). The background magnetic field B_0 is in the positive x direction. The code solves the following equations:

$$\frac{d\mathbf{x}_p}{dt} = \mathbf{v}_p,\tag{1}$$

$$m_p \frac{d\mathbf{v}_p}{dt} = e(\mathbf{E} + \frac{1}{c}[\mathbf{v}_p \times \mathbf{B}]), \tag{2}$$

$$\frac{1}{c}\frac{\partial \mathbf{B}}{\partial t} = -\nabla \times \mathbf{E},\tag{3}$$

$$\boldsymbol{E} = \frac{1}{c} [\boldsymbol{B} \times \boldsymbol{V}_e] - \frac{1}{e n_e} \nabla P_e, \tag{4}$$

$$\nabla \times \mathbf{B} = \frac{4\pi}{c} \mathbf{J},\tag{5}$$

$$\boldsymbol{J} = e(n_p \boldsymbol{V}_p - n_e \boldsymbol{V}_e), \tag{6}$$

where $n_e = n_p$. The quantities \mathbf{x}_p and \mathbf{v}_p are the positions and velocities of individual protons and \mathbf{V}_e is the electron bulk velocity. The proton number density n_p and bulk velocity \mathbf{V}_p for each spatial cell are calculated as moments of the distribution. The value m_p is the proton mass, e the elementary electric charge, e the speed of light, e time, e the electron number density, e the electric field, e the electron plasma pressure, and e the current density. The lengths of the simulation box in the directions parallel and perpendicular to e are e and e are e are e and e are e are e and e are e are e and e and e are e and e are e and e are e and e are e are e and e are e are e and e are e and e are e are e and e are e and e are e and e are e and e are e are e and e are e are e and e are e and e are e and e are e are e and e are e and e are e are e and e and e are e and e are e are e and e are e are e and e are e and e and e are e and e are e and e are e and e are e are e and e are e and e are e are e and e are e and e are e are e and e are e are e are e and e are e are e are e are e are e are e and e are e ar

This paper considers run IVb in Vasquez (2015) as a starting point, but an isothermal electron pressure is also included. In this run, the grid has 256^3 cells. Along the x direction the grid length L_{\parallel} , normalized by proton inertial lengths V_A/Ω_p , is 142.16, where V_A is the background Alfvén speed and Ω_p is the proton gyrofrequency. Along the perpendicular directions y and z, the grid length L_{\perp} is 25.13 so that the aspect ratio of the grid L_{\parallel}/L_{\perp} is 5.66. Triply periodic boundary conditions are used.

The initial proton plasma has a uniform density n_{p0} with 200 particles per cell. In the present analysis, the total β considered is unity. The total magnetic helicity signature is mainly a function of total β so results are similar regardless of how the ratio of proton to magnetic magnetic pressure β_p and ratio of electron to magnetic pressure β_e are individually assigned (Markovskii & Vasquez 2016). Here β_p is set to 0.2, for which 200 particles per cell yield accurate results, and β_e is set to 0.8. These plasma conditions can occur in slow winds. Significant magnetic helicity signatures are found to be present in the work

of Vasquez et al. (2018) for fluctuations in both slow and fast winds.

The initial fluctuations are energized at the lowest modes and have fluctuating bulk velocities and magnetic fields in accord with Alfvén waves. The initial proton distribution is a Maxwellian about the spatially varying bulk velocity. The initial rms of the combined average of the velocity fluctuations and magnetic field fluctuations in Alfvén units is $0.17\ V_A^2$. The developed turbulence is freely decaying.

The magnetic field fluctuations at t = 0 are given by the formula

$$\delta \mathbf{B}(0, \mathbf{x}) = \sum_{\mathbf{k}} [\tilde{\mathbf{B}}(0, \mathbf{k}) \times \cos(\mathbf{k} \cdot \mathbf{x} + \phi(\mathbf{k}))], \tag{7}$$

where x is a Cartesian spatial position vector, k is a wavevector, and $\phi(\mathbf{k})$ is a random phase uniformly assigned between 0 and 2π . Here the components of the vectors $\tilde{\bf B}$ obey the polarization relations of linear Alfvén waves in the MHD limit. The seed spectrum is confined to the modes on the surface of a cuboid with a combination of wavenumbers chosen from the set $(k_x=0,~\pm 2\pi/L_\parallel,~k_y=0,~\pm 2\pi/L_\perp,~k_z=0,$ $\pm 2\pi/L_{\perp}$), with all modes having the same amplitude except that the parallel and antiparallel propagating modes with $k_y = k_z = 0$ are given zero amplitude so as to exclude them from the initial state. The proton bulk velocity fluctuation δV is defined in the same way as $\delta \mathbf{B}$ in Equation (7), where $\tilde{\mathbf{V}}(0, \mathbf{k}) = -\operatorname{sign}(k_x) F[\operatorname{sign}(k_x)] \tilde{\mathbf{B}} \quad (0, \mathbf{k}) / (4\pi n_{p0} m_p)^{1/2} \quad \text{for}$ either $\tilde{V}(0, k_x = 0, k_y \neq 0, k_z) = -\operatorname{sign}(k_y)F[\operatorname{sign}(k_y)]$ $\tilde{\mathbf{B}}(0, k_x = 0, k_y \neq 0, k_z)/(4\pi n_{p0} m_p)^{1/2}$ or $\tilde{V}(0, k_x = 0, k_y = 0, k_z) = -\operatorname{sign}(k_z) F[\operatorname{sign}(k_z)]$ $\tilde{\mathbf{B}}(0, k_x = 0, k_y = 0, k_z)/(4\pi n_{p0} m_p)^{1/2}$ applies for $k_x = 0$. The function F[sign(k)] is assigned based on the initial value of σ_c . For $\sigma_c \ge 0$, $F = (1 - |\sigma_c|)/(1 + \sigma_c|)$ for sign(k) > 0 and F = 1for sign(k) < 0. The opposite assignment for F is used for $\sigma_{\rm c} < 0$.

3. Analysis of Spectral Magnetic Helicity

In accord with Vasquez (2015), the initial fluctuations develop a turbulent energy cascade and reach a quasi-steady state wherein the proton heating rate is nearly constant and both inertial and kinetic ranges are formed. (During the interval to be examined, the change in β_p is found to be limited to 0.02.) The magnetic helicity will be evaluated during the quasi-steady phase. In particular, the behavior of peak $|\sigma_{\rm m}|$ as a function of $|\sigma_{\rm c}|$ will be sought.

A nonzero initial value of rms $|\sigma_c|$ is needed, in general, to obtain a net magnetic helicity signature. The rms cross helicity is given by the formula:

$$\sigma_{\rm c} = 2 \frac{\sqrt{4\pi m_{\rm p} n_{p0}} (\delta \boldsymbol{V} \cdot \delta \boldsymbol{B})^{\rm avg}}{(4\pi m_{\rm p} n_{p0} |\delta \boldsymbol{V}|^2 + |\delta \boldsymbol{B}|^2)^{\rm avg}}.$$
 (8)

In Equation (8), the superscript "avg" denotes averaging over the grid and n_{p0} is again the uniform background proton number density. The vectors δV and δB are the fluctuating proton bulk velocity and magnetic field, respectively. The cross helicity is taken from the volume average, by definition, in MHD and is a rugged invariant for incompressible and constant

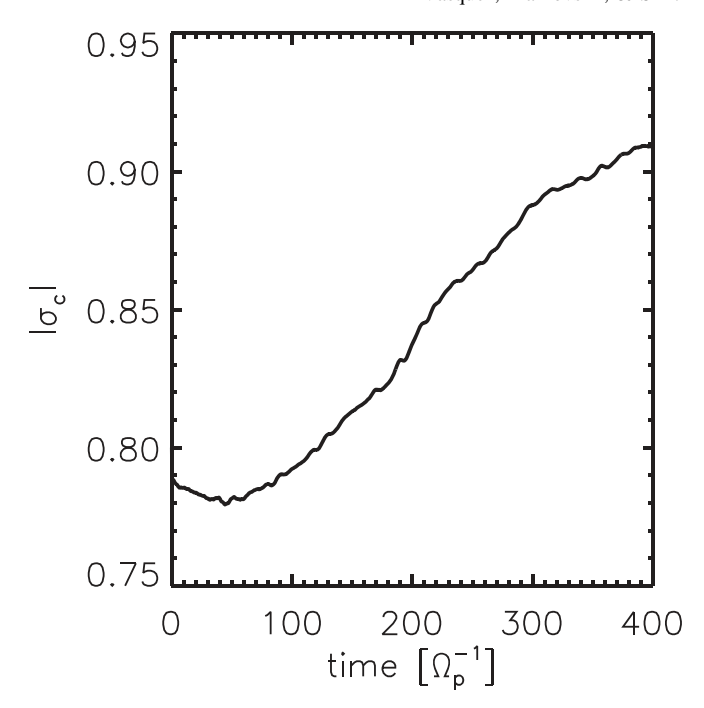


Figure 1. Plot of the magnitude of the normalized cross helicity $|\sigma_{\rm c}|$ as a function of time. The turbulent phase begins after t=160. The increase in $|\sigma_{\rm c}|$ is a nonlinear effect also found in MHD simulations.

density media. The formulation in Equation (8) is also used for spacecraft studies.

With a homogeneous background, the magnitude of rms $|\sigma_c|$ associated with the MHD-scale turbulent fluctuations increases with time and tends toward unity. This is due to nonlinear interactions (e.g., Matthaeus et al. 1983). Figure 1 shows an example. Therefore, the reference $|\sigma_c|$ value for time intervals to be defined further below, where the spectral magnetic helicity is obtained, will be calculated from the time average of $|\sigma_c|$ during those intervals.

From simulations, a normalized spectrum of $\sigma_{m,\text{tot}}$ is calculated according to

$$\sigma_{m,\text{tot}}(k_{\perp}) = k_{\perp} \frac{\langle \tilde{A} \cdot \tilde{B}^* \rangle}{\langle P_B \rangle}.$$
 (9)

In Equation (9), $\tilde{\pmb{B}}$ is the Fourier transform of the magnetic field, $\tilde{\pmb{B}}^*$ is the complex conjugate of $\tilde{\pmb{B}}$, $\tilde{\pmb{A}}$ is the Fourier transform of the vector potential determined from $\tilde{\pmb{B}} = i\pmb{k} \times \tilde{\pmb{A}}$ and the Coulomb gauge, the dot denotes a scalar product of complex vectors, and the brackets denote averaging over all perpendicular directions and parallel wavenumbers at a fixed perpendicular wavenumber k_{\perp} .

The normalized reduced magnetic helicity spectrum is calculated from the off-diagonal $\langle B_T B_N \rangle$ component (Matthaeus et al. 1982)

$$\sigma_{m,\text{red}}(k) = 2 \text{ Im}[\langle \tilde{B}_T^* \tilde{B}_N \rangle] / P_B,$$
 (10)

where k is the wavenumber of measured \boldsymbol{B} in the RTN coordinate system at some integral lag of the sample space. For the simulation $\hat{\boldsymbol{R}}$ is taken to be along the sampling path of a putative probe. Paths are chosen that are oblique to the direction of \boldsymbol{B}_0 , which is along the $\hat{\boldsymbol{x}}$ direction, and are characterized by an obliquity θ_B . These paths cross the grid just once from one side to another and are confined to the xy plane

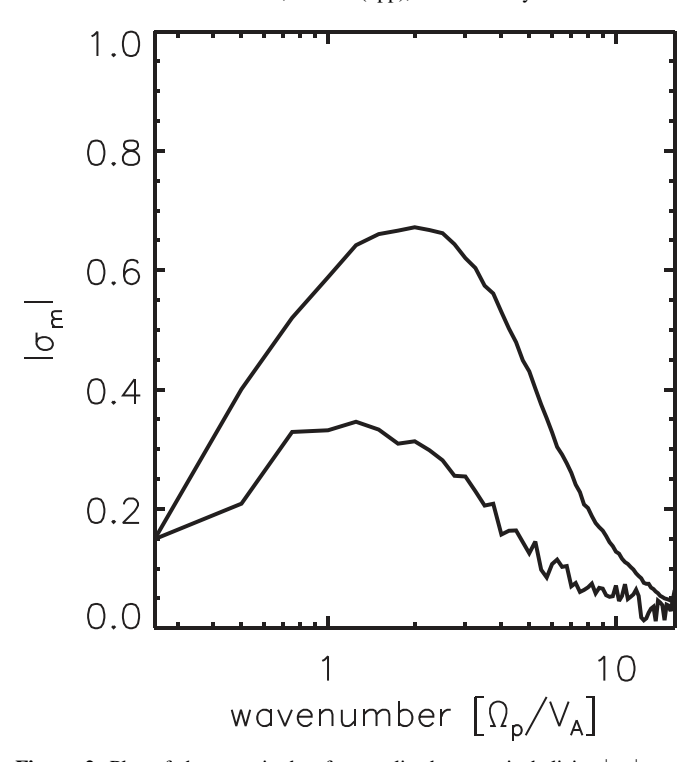


Figure 2. Plot of the magnitude of normalized magnetic helicity $|\sigma_{\rm m}|$ as a function of wavenumber. The upper curve is the magnetic helicity as a function of perpendicular wavenumber k_{\perp} integrated over k_{\parallel} . The lower curve is the reduced magnetic helicity for sample trajectories at 56° as a function of $k/\cos 56^\circ$ where k is the wavenumber along the sampling direction. The peak reduced magnetic helicity is 0.34.

of the simulation. Fields are sampled with 256 equally spaced measurements at fixed time so that the finite speed of the probe relative to the medium is neglected which is a good approximation for the solar wind at 1 au. B_N is assigned to the \hat{z} direction, and B_T completes a right-handed coordinate system. For a fixed θ_B , this process is repeated for many different lines ($\sim 10^5$) and for a range of times during the quasi-steady turbulent phase, and the final result is the average of all. With 3D results, many lines are readily available. The restriction of lines to the xy plane has been made so that the results can be computed in parallel using a spatial decomposition of the grid long the z direction.

Figure 2 shows the magnetic helicity for the same case as Figure 1 where the helicity is averaged from t=300–400, where t is normalized by Ω_p . The upper curve corresponds to $|\sigma_{m,\text{tot}}|$ and is plotted as a function of perpendicular wavenumber k_{\perp} . The signature is approximately Gaussian and reaches a peak of 0.68 near $k_{\perp}=2$. The lower curve is a reduced spectrum $|\sigma_{m,\text{red}}|$ taken by assuming that $\theta_B=56^\circ$, which is the mean angle of the interplanetary magnetic field at 1 au. It is shown as a function of $k/\cos 56^\circ$ where k is the projected wavenumber along a sampling path. The peak of the reduced spectrum is one-half of the total. In both cases, the helicity is found to have a right-handed sense assuming outward propagation.

A number of runs have been made to assess how peak $|\sigma_{m,\text{tot}}|$ and $|\sigma_{m,\text{red}}|$ values vary with concurrent $|\sigma_c|$ and the initial configuration of the fluctuations. Table 1 lists all the runs. In each run, two averaging time intervals have been considered: t=200–300 denoted by "a" following the case number and

 Table 1

 Parameters of the Simulation Runs

Case	$ \sigma_{m,\mathrm{tot}} $	$ \sigma_{m,\mathrm{red}} $	$ \sigma_c $
1a	0.38 ± 0.02	0.15 ± 0.03	0.38 ± 0.03
1b	0.39 ± 0.01	0.14 ± 0.02	0.45 ± 0.03
2a	0.46 ± 0.02	0.21 ± 0.02	0.61 ± 0.04
2b	0.56 ± 0.02	0.24 ± 0.02	0.69 ± 0.04
3a	0.57 ± 0.02	0.27 ± 0.03	0.87 ± 0.02
3b	0.68 ± 0.01	0.34 ± 0.01	0.90 ± 0.01
4a	0.57 ± 0.02	0.29 ± 0.02	0.88 ± 0.02
4b	0.64 ± 0.01	0.33 ± 0.02	0.91 ± 0.01
5a	0.50 ± 0.01	0.24 ± 0.01	0.88 ± 0.02
5b	0.59 ± 0.01	0.28 ± 0.02	0.91 ± 0.01
6a	0.42 ± 0.03	0.19 ± 0.01	0.82 ± 0.01
6b	0.46 ± 0.03	0.19 ± 0.01	0.84 ± 0.01

Note. Cases 1–3 differ only by the starting value of $|\sigma_c|$, which is 0.3, 0.5, and 0.8 respectively. Cases 3–5 differ only with respect to the random phases assigned to the initial fluctuations. Case 6 differs only from three having $L_{\parallel}=71.08$, which is one-half of that in case 3. The "a" on the case number denotes values obtained from t=200-300, whereas "b" from t=300-400.

t = 300 and 400 denoted by "b," each with a time cadence of 20. The reduced helicity is calculated for $\theta_B = 56^{\circ}$. Other θ_B are discussed briefly.

To determine the value of the magnetic helicity, both total and reduced, at the peak of a signature, the spectrum is fitted to an analytical function using the least squares procedure:

$$|\sigma_m| = C_1 \exp\left[-\frac{1}{2} \left(\frac{k - C_2}{C_3}\right)^2\right] + C_4 + C_5 k + C_6 k^2, \tag{11}$$

where C_i are the fitting constants and k is the relevant wavenumber. This combination of a Gaussian and a quadratic has proven to be a simple and accurate expression for an observed spectrum with a peak (Markovskii et al. 2015). Both the maximum and its position are taken from the fit function. In the observations of Markovskii et al. (2015) spectra included 65,384 samples so that low and high frequencies are in abundance. With just 256 samples in the simulated spectra, resolution at low wavenumbers can require restricting the fit to just a portion of the wavenumbers up to some maximum k beyond the position of the peak. For each case, the goodness of the fit has been examined and steps have been taken to make certain that the fit is appropriate.

Figure 3 plots $|\sigma_{m,\mathrm{red}}|$ as a function of $|\sigma_c|$ from data listed in Table 1, which also gives the peak value of $|\sigma_{m,\mathrm{tot}}|$ for comparison. The peak value is determined from the fit function. For each peak value, uncertainty lines are assigned in the horizontal direction based on the range of $|\sigma_c|$ over which the time average for the magnetic helicity was acquired. Uncertainty lines in the vertical direction pertain to the range of measured $|\sigma_{m,\mathrm{red}}|$ about the fit function peak of $|\sigma_{m,\mathrm{red}}|$ as a

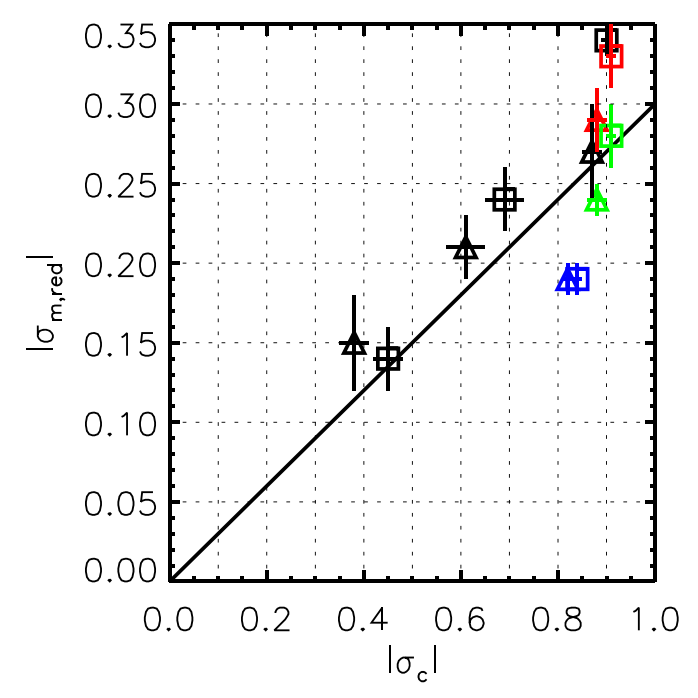


Figure 3. Plot of peak value of $|\sigma_{m,red}|$ as a function of $|\sigma_c|$ from the simulation-derived values listed in Table 1. The diagonal line is the fit of mean-observed values from WIND spacecraft data. Subscript "a" values are plotted as triangles and subscript "b" values as squares. Black lines are used for cases 1–3, red lines for case 4, green for case 5, and blue for case 6.

function of k. The solid line is the observed trend line of values from Vasquez et al. (2018).

Table 1 lists six cases. Cases 1–3 differ only by the starting value of $|\sigma_c|$, which is 0.3, 0.5, and 0.8, respectively. Cases 3–5 differ only with respect to the random phases assigned to the initial fluctuations. Case 6 only differs from case 3 by having $L_{\parallel}=71.08$, which is one-half of that in case 3. In case 6, the least oblique angle for the initial fluctuations is 71° and for case 3 it is 80°. As such, the initial fluctuations wavevectors are spread more widely about the perpendicular direction in case 6.

Values from cases 1–3 follow a trend with $|\sigma_c|$ that is consistent with the observed trend. At the highest $|\sigma_c| \sim 0.8$, cases 3–6 show a range of $|\sigma_{m,\mathrm{red}}|$ values. Values here can exceed 0.3 which is the maximum of observed trend as found in the one 2D case considered in Vasquez et al. (2018). During the same run, $|\sigma_{m,\mathrm{red}}|$ can rise or fall with time, even though $|\sigma_c|$ always increases. When only the initial phases differ between runs, different $|\sigma_{m,\mathrm{red}}|$ can also be found. For case 6 with a different initial wavevector distribution, the values are well below the trend line. The range of values about the observed trend line is significant and consistent with observed cases. From Table 1 similar variability occurs for $|\sigma_{m,\mathrm{tot}}|$. On average the ratio of $|\sigma_{m,\mathrm{red}}|$ to $|\sigma_{m,\mathrm{tot}}|$ in Table 1 is 0.45.

The influence of the initial phases of the fluctuations has been shown to affect the magnitude of the peak magnetic helicity in the developed dissipation range. Different initial conditions can generate a different superposition of fluctuations that interact nonlinearly with one another. This could influence the magnitude of the compressive and polarization properties that occur as a part of this superposition and so alter the magnetic helicity. However, the detailed reason for this outcome has not been identified.

When less oblique wavevectors are also included in simulations, the magnitude of the peak magnetic helicity is

also affected. The change between case 3 and 6 is consistent with propagating wave modes. The magnitude of magnetic helicity for kinetic Alfvén waves is greatest when propagating nearly perpendicular to B_0 . At lesser oblique angles, the helicity decreases and the polarization of the kinetic Alfvén wave approaches more closely a linear polarization with a smaller fluctuating parallel magnetic field component.

Restricted relations involving θ_B and $|\sigma_c|$ have been found for some cases. When the initial phases among the fluctuations are maintained, as in cases 1–3, the approximate relation $|\sigma_{m,\mathrm{red}}| = 0.68 |\sigma_c| \sin^2 \theta_B$ has been obtained. However, this relation does not always hold when the initial phases of the fluctuations are altered in the runs, such as for case 5. Differences apply both to the total and reduced magnetic helicity. This analysis shows that the magnetic helicity does not form a signature that is a strict function of $|\sigma_c|$. Instead initial conditions affect the values, and ensemble averaging, as performed with observations, results in a range of values that only possesses a mean trend with $|\sigma_c|$.

4. Discussion and Summary

The 3D hybrid simulations with fixed β have shown that the peak values of $|\sigma_{m,\text{tot}}|$ and $|\sigma_{m,\text{red}}|$ vary with fluctuation properties. They do not change as an exact one-to-one function of $|\sigma_c|$, although there is a significant trend with $|\sigma_c|$. Different initial phases among the fluctuations and a different wavevector configuration can alter the peak values obtained. There is an intrinsic variability present based on the initial fluctuation conditions. The variability is found among the different cases conducted, regardless of whether a total magnetic helicity or reduced magnetic helicity is evaluated. The reduced magnetic helicity is found to be nearly one-half of the total helicity in the runs conducted.

With intrinsic variability in the helicity peak values, a single simulation run cannot provide a suitable ensemble average of $|\sigma_{m,\mathrm{red}}|$ at a fixed value of $|\sigma_c|$ so as to match the observed mean. This can explain why the averaged reduced helicity taken from a single 2D run that was analyzed in Vasquez et al. (2018) did not give a result that matched the expected mean. Only when the initial assignment of fluctuations phases or wavevectors are varied in different runs, does a significant variation about the expected mean value occur. Here the ensemble averaging truly needs to span different initial conditions with respect to the fluctuations. Runs in 3D provide more phase space to explore than 2D runs in this manner, but clearly there is a computation expense to consider when doing so.

Values of $|\sigma_{m,red}|$ from many solar wind intervals were examined in Vasquez et al. (2018). Wavelets showed an advantage over the Blackman–Tukey spectral method by having less scatter about the mean trend with $|\sigma_c|$. With wavelets an arithmetic average over time was used to determine a net spectra signature from which the peak was determined. This straightforward averaging procedure is suggested here to be the source of the method's advantage. The helicity signature can be expected to vary along the sampling path taken by the spacecraft. Spectra in Vasquez et al. (2018) spanned about 3 correlation lengths and so different initial fluctuation conditions. This variability is also augmented by the changes in θ_B and β in subintervals that were demonstrated in Vasquez et al. (2018).

B.V. and S.M. were supported by the NASA Solar and Heliospheric Physics grants 80NSSC19K0832 and 80NSSC21K1674 to the University of New Hampshire (UNH). B.V. and C.S. were supported by NSF SHINE grant AGS1622413 and the NASA Heliophysics Grand Challenge Research grant 80NSSC17K0009 to UNH. C.S. was further supported by the Advanced Composition Explorer mission. The simulation results were obtained from the Cray XE6m-200 supercomputer Trillian at UNH. Trillian was purchased and administered with the support of NSF MRI grant PHYS-1229408 to UNH.

ORCID iDs

Bernard J. Vasquez https://orcid.org/0000-0001-8593-7289 Charles W. Smith https://orcid.org/0000-0002-5379-1542

References

```
Bruno, R., & Telloni, D. 2015, ApJL, 811, L17
Hamilton, K., Smith, C. W., Vasquez, B. J., & Leamon, R. J. 2008, JGRA, 113, A01106
He, J., Marsch, E., Tu, C., Yao, S., & Tian, H. 2011, ApJ, 731, 85
He, J., Tu, C., Marsch, E., & Yao, S. 2012, ApJ, 749, 86
Howes, G. G., & Quataert, E. 2010, ApJL, 709, L49
```

```
Klein, K. G., Howes, G. G., TenBarge, J. M., & Podesta, J. J. 2014, ApJ,
  785, 138
Leamon, R. J., Matthaeus, W. H., Smith, C. W., & Wong, H. K. 1998, ApJL,
  507, L181
Markovskii, S. A., & Vasquez, B. J. 2013a, ApJ, 768, 62
Markovskii, S. A., & Vasquez, B. J. 2013b, in AIP Conf. Proc. 153, 13th Int.
  Solar Wind Conf., ed. G. Zank et al. (Melville, NY: AIP), 239
Markovskii, S. A., & Vasquez, B. J. 2016, ApJ, 820, 15
Markovskii, S. A., Vasquez, B. J., & Smith, C. W. 2015, ApJ, 806, 78
Markovskii, S. A., Vasquez, B. J., & Smith, C. W. 2016, ApJ, 833, 212
Matthaeus, W. H., Goldstein, M. L., & Smith, C. W. 1982, PhRvL, 48, 1256
Matthaeus, W. H., Montogomery, D. C., & Goldstein, M. L. 1983, PhRvL,
  51, 1484
Podesta, J. J., & Gary, S. P. 2011, ApJ, 734, 15
Smith, C. W., Goldstein, M. L., & Matthaeus, W. H. 1983, JGR, 88, 5581
Smith, C. W., Goldstein, M. L., Matthaeus, W. H., & Viñas, A. F. 1984, JGR,
  89, 9159
Smith, C. W., Vasquez, B. J., & Hollweg, J. V. 2012, ApJ, 745, 8
Terasawa, T., Hoshino, M., Sakai, J.-I., & Hada, T. 1986, JGR, 91, 4171
Vasquez, B. J. 1995, JGR, 100, 1779
Vasquez, B. J. 2015, ApJ, 806, 33
Vasquez, B. J., & Markovskii, S. A. 2012, ApJ, 747, 19
Vasquez, B. J., Markovskii, S. A., & Chandran, B. D. G. 2014, ApJ, 788, 178
Vasquez, B. J., Markovskii, S. A., & Smith, C. W. 2018, ApJ, 855, 121
Woodham, L. D., Wicks, R. T., Verscharen, D., Owen, C. J., Maruca, B. A., &
   Alterman, B. L. 2019, ApJL, 884, L53
Zhao, G. Q., Lin, Y., Wang, X. Y., et al. 2021, ApJ, 906, 123
```